



# Empirical and Numerical Modelling of Gas–Gas Diffusion for Binary Hydrogen–Methane Systems at Underground Gas Storage Conditions

Sebastian Hogeweg<sup>1</sup> · Julia Michelsen<sup>1</sup> · Birger Hagemann<sup>1</sup> · Leonhard Ganzer<sup>1</sup>

Received: 3 June 2023 / Accepted: 5 November 2023 / Published online: 1 December 2023  
© The Author(s) 2023

## Abstract

The physical process in which a substance moves from a location with a higher concentration to a location with a lower concentration is known as molecular diffusion. It plays a crucial role during the mixing process between different gases in porous media. Due to the petrophysical properties of the porous medium, the diffusion process occurs slower than in bulk, and the overall process is also affected by thermodynamic conditions. The complexity of measuring gas–gas diffusion in porous media at increased pressure and temperature resulted in significant gaps in data availability for modelling this process. Therefore, correlations for ambient conditions and simplified diffusivity models have been used for modelling purposes. In this study, correlations in dependency of petrophysical and thermodynamic properties were developed based on more than 30 measurements of the molecular diffusion of the binary system hydrogen–methane in gas storage rock samples at typical subsurface conditions. It allows reproducing the laboratory observations by evaluating the bulk diffusion coefficient and the tortuosity factor with relative errors of less than 50 % with minor exceptions, leading to a strong improvement compared to existing correlations. The developed correlation was implemented in the open-source simulator DuMu<sup>x</sup> and the implementation was validated by reproducing the measurement results. The validated implementation in DuMu<sup>x</sup> allows to model scenarios such as Underground Hydrogen Storage (UHS) on a field-scale and, as a result, can be used to estimate the temporary loss of hydrogen into the cushion gas and the purity of withdrawn gas due to the gas–gas mixing process.

---

✉ Sebastian Hogeweg  
alexander.sebastian.hogeweg@tu-clausthal.de

Julia Michelsen  
julia.michelsen@tu-clausthal.de

Birger Hagemann  
birger.hagemann@tu-clausthal.de

Leonhard Ganzer  
leonhard.ganzer@tu-clausthal.de

<sup>1</sup> Institute of Subsurface Energy Systems, Clausthal University of Technology, Agricolastraße 10, Clausthal-Zellerfeld, Lower-Saxony 38678, Germany

## Article Highlights

- Development of a correlation for effective binary diffusion coefficients for the system  $\text{H}_2 - \text{CH}_4$  in porous media
- Depending on petrophysical and thermodynamic properties, this correlation is valid for typical subsurface conditions
- Implementation of the correlation in the open-source simulator DuMu<sup>x</sup> for reproduction and validation purposes

**Keywords** Molecular diffusion · Gas mixing in porous media · Underground hydrogen storage

## 1 Introduction

Gas–gas mixing in porous media is a complex process mainly governed by molecular diffusion and mechanical dispersion. Molecular diffusion can be defined as the flux caused by the general tendency of balancing concentration differences due to the Brownian motion of the molecules (Brown 1828; Fick 1855). In contrast, mechanical dispersion originates from the complexity of a porous medium and the resulting different lengths of flow paths and varying flow velocities. From the modelling background, the overall two-component flow can be expressed by the advection–diffusion term:

$$\frac{\partial c}{\partial t} = \underbrace{\nabla \cdot (D \nabla c)}_{\text{diffusive/dispersive term}} - \underbrace{\nabla \cdot (\mathbf{v}c)}_{\text{advection term}} + R \quad (1)$$

where  $c$  is the concentration,  $D$  is the diffusivity/dispersivity,  $\mathbf{v}$  is the velocity field, and  $R$  is the source term. Focusing on the isothermal fluid flow, the flow velocity in porous media  $\mathbf{v}$  is pressure controlled and typically expressed by Darcy's Law (Darcy 1856). Contrarily, the molecular diffusive term is governed by concentration gradients, which reasonably reflects the natural tendency to balance the concentrations. This phenomenon of molecular diffusion is described by Fick's first law (Fick 1855):

$$J_D^\kappa = -\rho D^\kappa \nabla c_g^\kappa \quad (2)$$

where  $J_D^\kappa$  is the diffusive flux of component  $\kappa$  in  $\text{mol}/(\text{m}^2 \cdot \text{s})$ ,  $\rho$  is the molar density in  $\text{mol}/\text{m}^3$ ,  $D^\kappa$  is the diffusion coefficient in  $\text{m}^2/\text{s}$ , and  $\nabla c_g^\kappa$  the concentration gradient (mole fraction) in the gaseous phase in  $1/\text{m}$ .

In the simplest case, a binary system can be considered. Here, it is evident that each component's flux must be balanced to conserve the material balance (Bear 2018).

$$\sum_{\kappa} J_D^\kappa = 0 \quad (3)$$

Fulfilling this condition, the diffusion coefficients of both components have to be identical:

$$D^A = D^B = D^{AB} \quad (4)$$

A recent approach of measuring bulk diffusion coefficients at higher temperatures ( $T = 19.4$  to  $59.7$  °C) and pressures ( $p = 90$  bar to  $147$  bar) for the binary system methane–carbon

dioxide was shown in Guevara-Carrion et al. (2019), where diffusion coefficients in the range of  $1.46\text{--}3.7 \cdot 10^{-8} \text{ m}^2/\text{s}$  were observed. To estimate gas–gas diffusion coefficients numerous correlations (e.g. Fuller’s method (Fuller et al. 1966) or Wilke’s method (Wilke and Lee 1955)) have been developed in the past, whereby they are typically limited to low pressure and temperature ranges. Therefore, these models have limited applicability to the conditions during the storage of gases in the porous subsurface. Furthermore, diffusion can only occur within the pores in porous media and is therefore decelerated compared to the open flow due to the reduced space for exchange. For the one-dimensional system, the flow pathway through the rock is extended due to the tortuosity of the pore structure. This reduction can be expressed as follows (Helmig 1997):

$$D_{\text{pm}}^{\text{AB}} = \phi \tau S_g D_{\text{bulk}}^{\text{AB}} \quad (5)$$

where  $D_{\text{pm}}^{\text{AB}}$  is the effective binary diffusion coefficient of the porous media in  $\text{m}^2/\text{s}$ ,  $\phi$  is the porosity,  $\tau$  is the tortuosity factor of the porous medium,  $S_g$  is the gas saturation, and  $D_{\text{bulk}}^{\text{AB}}$  is the binary diffusion coefficient for the bulk medium in  $\text{m}^2/\text{s}$ .

So far, only few measurements of effective diffusion coefficients in porous media have been conducted. Pandey et al. (1974) and Chen et al. (1977) performed steady state and unsteady state measurements at pressures up to 5 bar. Pandey et al. (1974) used a steady state method for dry samples, while for saturated and low permeable samples an unsteady state measurement method was selected. Here, effective diffusion coefficients for the binary system He- $\text{N}_2$  in the range of  $2.14 \cdot 10^{-6} \text{ m}^2/\text{s}$  to  $1.19 \cdot 10^{-4} \text{ m}^2/\text{s}$  (steady state method) and  $1.67 \cdot 10^{-8} \text{ m}^2/\text{s}$  to  $1.88 \cdot 10^{-5} \text{ m}^2/\text{s}$  (unsteady state method) were measured. Chen et al. (1977) observed higher diffusion coefficients ( $2.59 \cdot 10^{-5}$  to  $2.00 \cdot 10^{-3} \text{ m}^2/\text{s}$ ) for  $\text{CH}_4\text{-N}_2$  at a pressure of  $p = 1$  bar and a temperature of  $T = 35 \text{ }^\circ\text{C}$ .

Overall, the lack of experimental data and insufficient characterisation of molecular diffusion at storage conditions leads to a knowledge gap which is addressed within this work. The goal of the present study is the development of a combination of correlations in the form of Eq. 6 representing the process of molecular diffusion between the two components hydrogen and methane as the main component of natural gas.

$$D_{\text{pm}}^{\text{AB}} = \phi \tau(\phi, S_g, k) S_g D_{\text{bulk}}^{\text{AB}}(p, T) \quad (6)$$

where  $p$  corresponds to the pore pressure in bar and  $T$  is the temperature in K.

Afterwards, the model is implemented in the open-source simulator DuMu<sup>x</sup> to calibrate the numerical model with respect to the forecast of UHS scenarios.

## 2 Empirical Correlation of Binary Diffusion Coefficients of $\text{H}_2\text{-CH}_4$ at High-Pressure and High-Temperature Conditions

To gain data on molecular diffusion coefficients, a total of 32 experiments have been conducted. The one-chamber method allows the measurement of effective binary diffusion coefficients of two gaseous components. In the following, the experimental procedure used to gain data for the modelling approach is briefly described. A more extensive description can be found in Michelsen et al. (2023).

## 2.1 Experimental Procedure of Measuring Gas–Gas Molecular Diffusion in the Laboratory

To measure molecular diffusion, a binary diffusion setup was used, which was adapted from the work of Wicke and Kallenbach (1941). The measurements were performed with a quasi-stationary one-chamber method.

The main component of the setup is a core holder, which is developed for rock samples with a length of up to 6 cm and a diameter of 3 cm, as depicted in Fig. 1. Before each experiment, the core samples are stored in the oven ( $T = 65\text{ }^{\circ}\text{C}$ ) to ensure that the samples do not contain any water. For the measurements involving gas saturations smaller unity, the sample is firstly fully water saturated, followed by the injection of nitrogen to displace the water partially and establish the two-phase saturation. The saturation in place is determined by weighting the partially and fully saturated sample.

The core holder, also known as the diffusion cell, consists of a hollow cylinder which contains a rock sample, one gas distribution element, one gas injection element, and two end pieces. The hollow cylinder serves as a large chamber and is located on one side of the rock sample. It must have a volume that is a multiple of the rock sample's volume. Before placing these components into the diffusion cell, they are inserted into a Viton sleeve. On the other side of the rock sample is the gas distribution element with an inlet and an outlet. Prior to the experiment, the water-filled annulus surrounding the Viton sleeve is slowly pressurised to build up a certain radial pressure on the core specimen. This radial pressure is greater than the measurement pore pressure of the gas. Simultaneously, the diffusion cell is filled and pressurised with hydrogen step-wise along with the radial pressure. During the experiment, methane is injected into the diffusion cell through the inlet, controlled by a syringe pump that drives a floating piston chamber. A backpressure regulator is installed at the outlet of the target to maintain a constant pressure in the diffusion cell during the measurement. The injection is continued until a clear trend (straight line) in the gas composition is identifiable. A gas chromatograph is situated behind the backpressure regulator which continuously analyses the gas composition.

The effective diffusion coefficients were determined by matching the measurement results with a one-dimensional numerical simulation model, which was implemented in COMSOL Multiphysics. The model solves the partial differential equation which corresponds to Fick's second law including the modification where the volume is reduced to the pore space. The one-dimensional domain representing the rock sample is discretised by 100 elements. The boundaries are defined as solution-dependent Dirichlet boundaries where the concentration of the chambers changes over time in dependency on the boundary fluxes. For chamber 1, the flushing of methane is considered additionally within the boundary condition. The matching of the simulated and measured hydrogen concentrations is done manually by changing the effective diffusion coefficient. A more

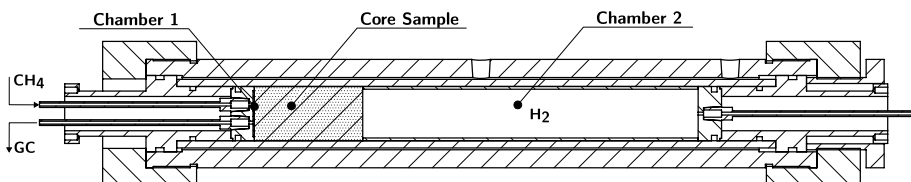


Fig. 1 Schematic representation of the diffusion cell

extensive description can be found in Michelsen et al. (2023), Michelsen et al. (2023) and an example of the COMSOL simulation can be found in the repository (Hogeweg et al. 2023).

## 2.2 Development of a Correlation for Molecular Diffusion in Porous Media

To develop a mathematical model characterising the diffusive flux of the binary system  $H_2$ - $CH_4$  in the subsurface, three data sets (Michelsen et al. 2023) of experiments are investigated. While a first set (see Table 1) contains various samples from actual storage formations (samples B to H) at the reference temperature and pore pressure conditions of  $T = 40\text{ }^\circ\text{C}$  and  $p = 100\text{ bar}$  isolating the dependency of the petrophysical properties of the porous media, the second set (cf. Table 2) is composed of the measurements performed on the reference sample A (Bentheimer Sandstone) at various thermodynamic conditions to establish the dependency of the diffusion coefficient on pressure and temperature. A final extended data set is used to validate and assess the accuracy of the developed correlation (see Tables 3 and 4).

Overall, the laboratory measurements show a dependency on the thermodynamic conditions and the influence of the petrophysical properties on the strength of the molecular diffusion. In general, the experimental observations indicate that the effective diffusion coefficient decreases with increasing temperature. In low-pressure ranges ( $< 75\text{ bar}$ ), the coefficient decreases with increasing pressure, followed by an increasing trend for higher pressures. Higher porosities, low water saturations, and higher permeabilities show a higher effective molecular diffusion coefficient.

### 2.2.1 Modelling of the Tortuosity Factor Representing the Influence of the Porous Medium

In the first step, the dependency of the diffusion coefficient on the properties of the porous media is analysed. Here, the data from Table 1 are used. The intention is to develop a correlation for the tortuosity factor in dependency of porosity, permeability, and gas saturation, as these parameters are typically already determined on investigations such as well logging,

**Table 1** Data Set 1 - Measurements at  $T = 40\text{ }^\circ\text{C}$  and  $p = 100\text{ bar}$

Sample	Porosity [-]	Permeability [mD]	Gas sat [-]	Eff. diff. coeff. [m <sup>2</sup> /s]
A	0.247	2500	0.4	$5.00 \times 10^{-9}$
A	0.247	2500	0.6	$4.00 \times 10^{-8}$
A	0.247	2500	1	$1.10 \times 10^{-7}$
B	0.299	71	1	$7.00 \times 10^{-8}$
C	0.268	157.6	1	$6.00 \times 10^{-8}$
D	0.317	718.6	1	$2.30 \times 10^{-7}$
E	0.199	23.6	1	$2.60 \times 10^{-8}$
F	0.321	288.2	1	$1.20 \times 10^{-7}$
G	0.274	263.1	1	$9.80 \times 10^{-8}$
H	0.176	17.2	1	$1.80 \times 10^{-8}$
I	0.210	105	1	$3.70 \times 10^{-8}$

routine core analysis (RCAL), and operation history. A straightforward trial and error approach leads to a satisfying result as depicted in Fig. 2. Merely one measurement point (sample D) deviates from the developed correlation. Here, diverging pore connectivity and topology of the sample on pore scale could explain the deviation. Nevertheless, the best match has the following form:

$$D_{pm}^{AB} = \phi^2 S_g^2 k_{eff}^{1/5} \cdot 3.785 \cdot 10^{-4} \tag{7}$$

where  $D_{pm}^{AB}$  is the binary diffusion coefficient between  $H_2-CH_4$  in  $m^2/s$ ,  $\phi$  is the porosity,  $S_g$  is the gas saturation, and  $k_{eff}$  is the effective permeability in  $m^2$ .

To isolate the tortuosity factor of the porous medium, the Fuller method (Fuller et al. 1966; Fuller and Giddings 1965; Fuller et al. 1969) is selected due to its reported good accuracy at low pressures and temperatures to describe the bulk diffusion coefficient. Evaluating Fuller’s method at  $T = 40 \text{ }^\circ\text{C}$  and  $p = 10 \text{ bar}$  ( $D_{bulk}^{AB} = 2.1395 \times 10^{-6} \text{ m}^2/\text{s}$ ) allows us to determine the tortuosity factor of the Bentheimer sample ( $\tau_A = 0.208$ ). In the general form, the first part of the correlation can be expressed as follows:

$$D_{pm}^{AB} = \phi S_g \tau D_{bulk}^{AB} \tag{8}$$

$$\text{HMHG}_{\text{poro}} : \quad \tau = \phi S_g k_{eff}^{1/5} \cdot 176.916 m^{-2/5} \tag{9}$$

### 2.2.2 Modelling the Impact of Pressure and Temperature on the Process of Molecular Diffusion

A mathematical model to describe the bulk diffusion coefficient in dependency on pressure and temperature is developed based on the correlation for the tortuosity factor. Here, a second degree (2x2y) polynomial regression of the second data set (see Table 2) is used to predict the effective diffusion coefficient (see Fig. 3). The impact of the porous medium can be eliminated with Eqs. (8–9). The best fit for the bulk diffusion coefficients in dependency of temperature and pressure is achieved with the following coefficients:

**Fig. 2** Developed correlation  $\text{HMHG}_{\text{poro}}$  of the effective diffusion coefficient based on various rock samples varying in petrophysical properties and saturation

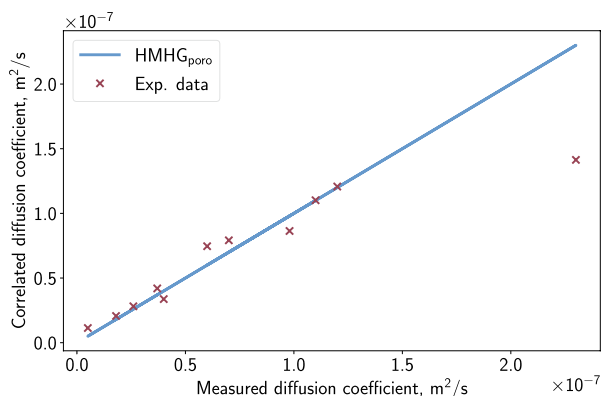
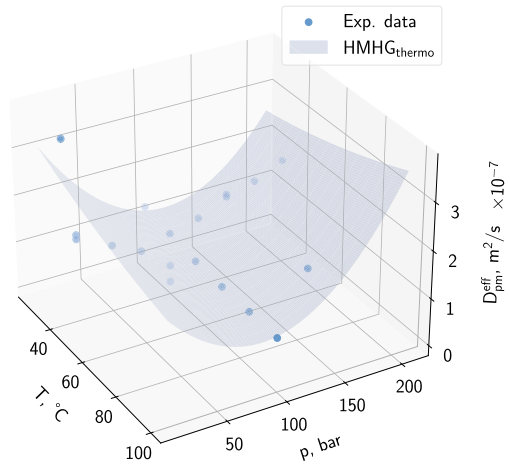


**Table 2** Data Set 2 - Measurements with constant petrophysical properties ( $\phi = 0.247$ ,  $k = 2500$  mD, and  $S_g = 1$ )

Sample	Temperature [°C]	Pressure [bar]	Eff. Diff. Coeff. [m <sup>2</sup> /s]
A	40	20	1.55×10 <sup>-7</sup>
A	40	20	1.64×10 <sup>-7</sup>
A	40	50	1.20×10 <sup>-7</sup>
A	40	75	9.00×10 <sup>-8</sup>
A	40	100	1.10×10 <sup>-7</sup>
A	40	125	1.26×10 <sup>-7</sup>
A	40	150	1.55×10 <sup>-7</sup>
A	40	150	1.60×10 <sup>-7</sup>
A	40	175	1.72×10 <sup>-7</sup>
A	40	200	2.00×10 <sup>-7</sup>
A	25	100	1.20×10 <sup>-7</sup>
A	55	100	1.00×10 <sup>-7</sup>
A	70	100	9.60×10 <sup>-8</sup>
A	85	100	9.50×10 <sup>-8</sup>
A	100	100	9.30×10 <sup>-8</sup>
A	85	150	1.49×10 <sup>-7</sup>
A	40	10	3.71×10 <sup>-7</sup>
A	40	10	3.70×10 <sup>-7</sup>

**Fig. 3** Effective diffusion coefficient as function of pressure and temperature of the Bentheimer Sandstone sample (sample A)



$$\text{HMHG}_{\text{thermo}} : D_{\text{bulk}}^{\text{AB}}(T, p) = \beta_1 + \beta_2 T + \beta_3 p + \beta_4 T^2 + \beta_5 T p + \beta_6 p^2 \quad (10)$$

$$\beta_1 = 3.61069 \times 10^{-5} \text{ m}^2/\text{s} \quad (11)$$

$$\beta_2 = -1.46672 \times 10^{-7} \text{ m}^2/(\text{K s}) \quad (12)$$

$$\beta_3 = -1.74842 \times 10^{-12} \text{ m}^2/(\text{Pa s}) \quad (13)$$

$$\beta_4 = 1.67793 \times 10^{-10} \text{ m}^2/(\text{K}^2 \text{ s}) \quad (14)$$

$$\beta_5 = 2.95155 \times 10^{-15} \text{ m}^2/(\text{Pa K s}) \quad (15)$$

$$\beta_6 = 3.71863 \times 10^{-20} \text{ m}^2/(\text{Pa}^2 \text{ s}) \quad (16)$$

Afterwards, the developed correlations (Eqs. 9, 10–16) can be merged into its final form of:

$$D_{\text{pm}}^{\text{AB}} = \phi \tau(\phi, S_g, k) S_g D_{\text{bulk}}^{\text{AB}}(p, T) \quad (17)$$

in terms of the new correlation:

$$D_{\text{pm}}^{\text{AB}} = \phi \text{HMHG}_{\text{poro}}(\phi, S_g, k) S_g \text{HMHG}_{\text{thermo}}(p, T) \quad (18)$$

## 2.3 Comparison to Existing Correlations and Estimation of Relative Error

The developed correlations (Eqs. 9, 10, and 18) are compared with existing models. Correlations for the tortuosity factor and the bulk diffusion coefficient are examined independently. Afterwards, the relative error of the developed and existing correlation sets is estimated and compared.

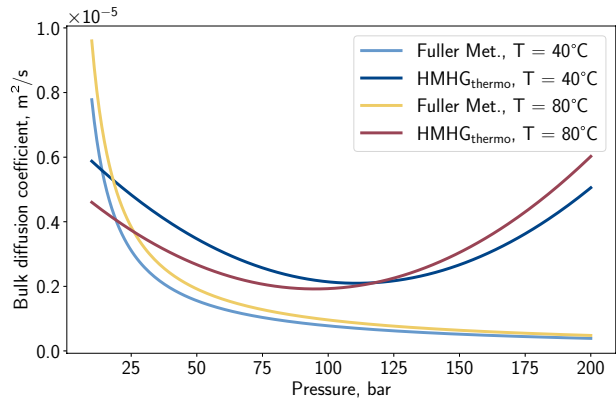
### 2.3.1 Bulk Binary Diffusion Coefficient

The difficulty of accurately measuring gas–gas bulk diffusion coefficients at higher temperatures and pressures leads to a limited number of correlations describing this parameter. A typical correlation is Fuller’s method (cf. Eq. 19) (Fuller and Giddings 1965; Fuller et al. 1966, 1969), which shows good accuracies in low-pressure range (< 10 bar) according to literature (Poling et al. 2001). An advantage of this correlation is the general formulation which enables the prediction of various binary combinations of components:

$$D_{\text{bulk}}^{\text{AB}} = \frac{0.0143T^{1.75}}{pM_{\text{AB}}^{0.5} \left( (\Sigma_v)_A^{1/3} + (\Sigma_v)_B^{1/3} \right)^2} \quad (19)$$



**Fig. 4** Comparison of bulk diffusion coefficients determined with Fuller’s method and the proposed correlation as function of pressure



$$M_{AB} = \frac{2}{\frac{1}{M_A} + \frac{1}{M_B}} \tag{20}$$

where  $D_{\text{bulk}}^{AB}$  is the bulk binary diffusion coefficient in  $\text{m}^2/\text{s}$ ,  $T$  is the temperature in K,  $p$  is the pressure in Pa,  $M_{AB}$  is the harmonic mean of the molecular weight of components A and B in  $\text{g/mol}$ , and  $\Sigma_v$  is the atomic diffusion volume.

Figure 4 depicts the trend of the bulk diffusion coefficient versus pressure according to Fuller’s method and the developed correlation. While Fuller’s method leads to a strongly monotonic decreasing diffusion coefficient with increasing pressure, the developed correlation leads to an initial decrease followed by an increasing diffusion coefficient. This yields consistent results at low-medium pressures ( $\approx 25$  bar), but the deviation between both models grows with increasing pressure. Based on the experimental investigations and developed correlation, the bulk diffusion coefficients seem to be higher than expected. According to the theory (Einstein 1905; Von Smoluchowski 1906), the behaviour as predicted by Fuller’s method is more reasonable than the correlation in the present study. However, Guevara-Carrion et al. (2019) described a similar trend as observed in the presented experiments. Guevara-Carrion et al. (2019) concluded that this phenomenon is caused by the transition between liquid-like to gas-like state within the supercritical region, which could also be applicable in the present study. Nevertheless, the measurement of the bulk diffusion coefficient in a similar experimental approach without a core specimen is recommended to determine experimentally the data point (see Sect. 2.2.1), which is currently based on Fuller’s method.

### 2.3.2 Tortuosity Factor

The commonly used model of Millington and Quirk (1961) is compared with the developed correlation for the tortuosity factor. The model of Millington & Quirk estimates the tortuosity factor of a porous medium based on its porosity and gas saturation (cf. Eq. 21). This leads to the situation that rock samples with large pores and tiny pore throats can possess the same tortuosity as specimens with comparatively small pores and big pore throats. Figure 5 compares the developed correlation for two different porosities. Both correlations generally show an increasing tortuosity factor with

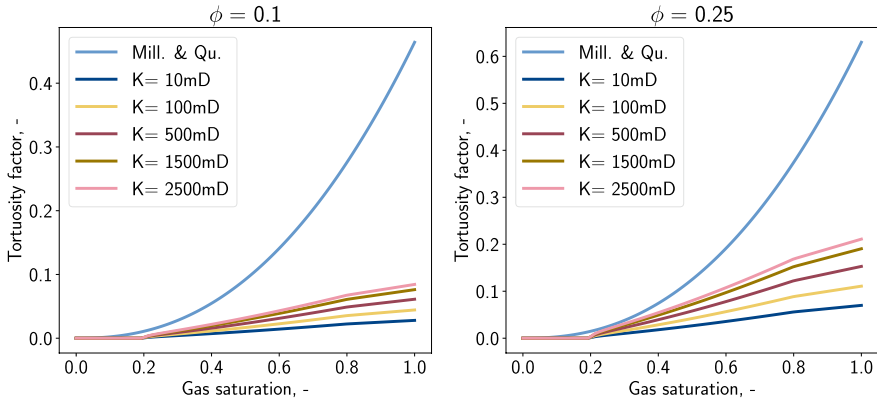


**Fig. 5** Comparison of tortuosity factor determined with Millington & Quirk and the proposed correlation as function of gas saturation, porosity, and absolute permeability. To determine the impact of relative permeability, the Brooks–Corey model (Brooks and Corey 1964) is used, parameterised with  $S_{wc} = 0.2$  and  $\lambda = 2$

increasing petrophysical properties and gas saturation. This is physically reasonable as the higher the tortuosity factor, the more it behaves as a bulk volume ( $\tau_{bulk} = 1$ ). Furthermore, with increasing saturation, the deviation between both models increases so that at high gas saturations, the tortuosity factor in the correlation is approximately 3 to 4 times lower than the result of the model of Millington & Quirk.

$$\tau = \phi^{1/3} S_g^{7/3} \tag{21}$$

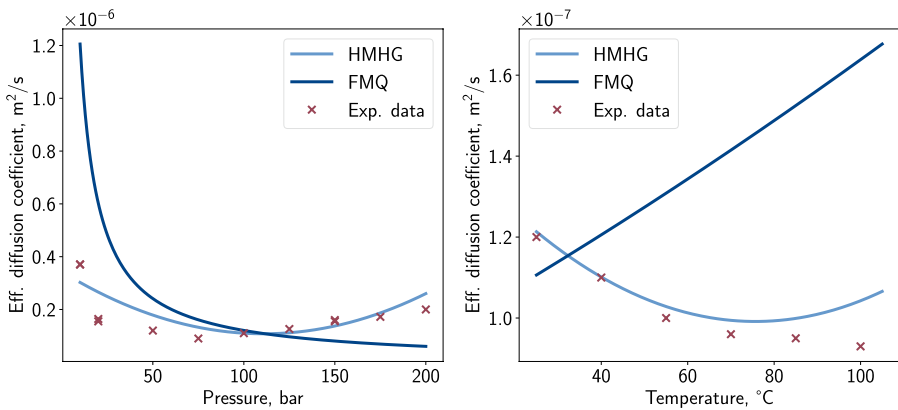


**Fig. 6** Comparison of correlated (model HMHG and FMQ) and measured effective diffusion coefficient of the porous media (sample A)

### 2.3.3 Overview of Correlated Effective Diffusion Coefficients and Error Analysis

With respect to the accuracy of the correlations, the correlated results of the proposed model (HMHG) and the established combination of Fuller’s method and Millington & Quirk (FMQ) to the laboratory observations are compared. Specifically, for the reference sample A, the comparison is depicted in Fig. 6. Regarding the pressure trend, the observations are analogous to Sect. 2.3.1 as it is only scaled by the product of the porosity, gas saturation, and the tortuosity factor of sample A. More interesting is the diverging trend of the diffusion coefficient with increasing temperatures. Here, the results of model FMQ shows an increasing quasilinear behaviour; while, the experimental observations indicate a decreasing trend. The general trend is reproduced by model HMHG, although at high temperatures, the deviation between measured and correlated coefficients is increasing. As an additional parameter of the accuracy of the models, the relative error is determined:

$$\delta_{D_{pm}^{AB}} = \frac{D_{pm}^{measured} - D_{pm}^{correlated}}{D_{pm}^{measured}} \tag{22}$$

**Table 3** Overview of the correlated diffusion coefficients—Model HMHG corresponds to proposed correlation of this study; while, model FMQ represents the combination of Fuller’s method and Millington & Quirk

Sample	Thermodynamic		Petrophysical properties			Effective diffusion coefficient $D_{pm}^{eff}$ , $m^2/s$			Relative error $\delta_{D_{pm}^{AB}}$ , %	
	$T$ , °C	$p$ , bar	$\phi$ , -	$k$ , mD	$S_g$ , -	Lab.	HMHG	FMQ	HMHG	FMQ
A	40	50	0.247	2500	1	$1.20 \times 10^{-7}$	$1.79 \times 10^{-7}$	$2.41 \times 10^{-7}$	-48.90	-100.91
A	40	75	0.247	2500	1	$9.00 \times 10^{-8}$	$1.32 \times 10^{-7}$	$1.61 \times 10^{-7}$	-47.16	-78.59
A	40	100	0.247	2500	1	$1.10 \times 10^{-7}$	$1.10 \times 10^{-7}$	$1.21 \times 10^{-7}$	-0.12	-9.59
A	40	125	0.247	2500	1	$1.26 \times 10^{-7}$	$1.12 \times 10^{-7}$	$9.64 \times 10^{-8}$	11.31	23.46
A	40	150	0.247	2500	1	$1.55 \times 10^{-7}$	$1.37 \times 10^{-7}$	$8.04 \times 10^{-8}$	11.43	48.15
A	40	150	0.247	2500	1	$1.60 \times 10^{-7}$	$1.37 \times 10^{-7}$	$8.04 \times 10^{-8}$	14.19	49.77
A	40	175	0.247	2500	1	$1.72 \times 10^{-7}$	$1.87 \times 10^{-7}$	$6.89 \times 10^{-8}$	-8.58	59.95
A	40	200	0.247	2500	1	$2.00 \times 10^{-7}$	$2.60 \times 10^{-7}$	$6.03 \times 10^{-8}$	-30.08	69.86
A	25	100	0.247	2500	1	$1.20 \times 10^{-7}$	$1.21 \times 10^{-7}$	$1.11 \times 10^{-7}$	-1.10	7.81
A	55	100	0.247	2500	1	$1.00 \times 10^{-7}$	$1.03 \times 10^{-7}$	$1.31 \times 10^{-7}$	-2.84	-30.83
A	70	100	0.247	2500	1	$9.60 \times 10^{-8}$	$9.94 \times 10^{-8}$	$1.41 \times 10^{-7}$	-3.57	-47.37
A	85	100	0.247	2500	1	$9.50 \times 10^{-8}$	$9.99 \times 10^{-8}$	$1.52 \times 10^{-7}$	-5.16	-60.50
A	100	100	0.247	2500	1	$9.30 \times 10^{-8}$	$1.04 \times 10^{-7}$	$1.64 \times 10^{-7}$	-12.11	-76.16
A	85	150	0.247	2500	1	$1.49 \times 10^{-7}$	$1.61 \times 10^{-7}$	$1.02 \times 10^{-7}$	-8.22	31.78
A	40	10	0.247	2500	1	$3.71 \times 10^{-7}$	$3.02 \times 10^{-7}$	$1.21 \times 10^{-6}$	18.48	-224.93
A	40	10	0.247	2500	1	$3.70 \times 10^{-7}$	$3.02 \times 10^{-7}$	$1.21 \times 10^{-6}$	18.26	-225.80
A	40	20	0.247	2500	1	$1.55 \times 10^{-7}$	$2.66 \times 10^{-7}$	$6.03 \times 10^{-7}$	-71.46	-288.86
A	40	20	0.247	2500	1	$1.64 \times 10^{-7}$	$2.66 \times 10^{-7}$	$6.03 \times 10^{-7}$	-62.05	-267.52
A	40	100	0.247	2500	0.4	$5.00 \times 10^{-9}$	$1.14 \times 10^{-8}$	$5.68 \times 10^{-9}$	-127.10	85.79
A	40	100	0.247	2500	0.6	$4.00 \times 10^{-8}$	$3.37 \times 10^{-8}$	$2.20 \times 10^{-8}$	15.72	-339.23

**Table 4** Overview of the correlated diffusion coefficients—Model HMHG corresponds to proposed correlation of this study; while, model FMQ represents the combination of Fuller’s method and Millington & Quirk

Sample	Thermodynamic		Petrophysical properties			Effective diffusion coefficient			Relative error	
	$T, ^\circ\text{C}$	$p, \text{bar}$	$\phi, -$	$k, \text{mD}$	$S_g, -$	$D_{pm}^{eff}, \text{m}^2/\text{s}$			$\delta_{D_{pm}^{AB}}, \%$	
						Lab.	HMHG	FMQ	HMHG	FMQ
B	40	100	0.299	71	1	$7.00 \times 10^{-8}$	$7.92 \times 10^{-8}$	$1.56 \times 10^{-7}$	-13.09	-122.17
B	50	106	0.299	71	1	$6.50 \times 10^{-8}$	$7.47 \times 10^{-8}$	$1.55 \times 10^{-7}$	-14.96	-138.49
C	40	100	0.299	157.6	1	$6.00 \times 10^{-8}$	$9.29 \times 10^{-8}$	$1.56 \times 10^{-7}$	-54.75	-159.20
C	25	53.5	0.268	157.6	1	$1.10 \times 10^{-7}$	$1.30 \times 10^{-7}$	$2.31 \times 10^{-7}$	-18.56	-109.58
D	40	100	0.317	718.6	1	$2.30 \times 10^{-7}$	$1.41 \times 10^{-7}$	$1.68 \times 10^{-7}$	38.54	26.90
D	45	88.3	0.317	718.6	1	$2.00 \times 10^{-7}$	$1.46 \times 10^{-7}$	$1.96 \times 10^{-7}$	26.93	2.12
E	40	100	0.199	23.6	1	$2.60 \times 10^{-8}$	$2.81 \times 10^{-8}$	$9.04 \times 10^{-8}$	-8.21	-247.58
E	107	140.5	0.199	23.6	1	$1.70 \times 10^{-8}$	$4.18 \times 10^{-8}$	$9.03 \times 10^{-8}$	-145.67	-431.21
F	40	100	0.321	288.2	1	$1.20 \times 10^{-7}$	$1.21 \times 10^{-7}$	$1.71 \times 10^{-7}$	-0.62	-42.47
F	86	116.5	0.321	288.2	1	$1.10 \times 10^{-7}$	$1.21 \times 10^{-7}$	$1.87 \times 10^{-7}$	-9.62	-69.57
G	40	100	0.274	27.4	1	$9.80 \times 10^{-8}$	$5.50 \times 10^{-8}$	$1.38 \times 10^{-7}$	43.93	-41.26
G	96	287.3	0.274	27.4	1	$1.70 \times 10^{-7}$	$4.27 \times 10^{-7}$	$6.43 \times 10^{-8}$	-151.15	62.19
H	40	100	0.176	17.2	1	$1.80 \times 10^{-8}$	$2.07 \times 10^{-8}$	$7.67 \times 10^{-8}$	-14.76	-326.23
H	92	203	0.176	17.2	1	$9.00 \times 10^{-9}$	$6.44 \times 10^{-8}$	$4.95 \times 10^{-8}$	-615.39	-449.46
I[1]	25	40	0.21	105	1	$1.15 \times 10^{-7}$	$8.77 \times 10^{-8}$	$2.23 \times 10^{-7}$	23.73	-93.70
I[1]	25	60	0.21	105	1	$6.50 \times 10^{-8}$	$6.81 \times 10^{-8}$	$1.49 \times 10^{-7}$	-4.78	-128.46
I[1]	40	100	0.21	105	1	$3.70 \times 10^{-8}$	$4.22 \times 10^{-8}$	$9.71 \times 10^{-8}$	-14.13	-162.41

[1] Berea sandstone sample

An overview of the corresponding results is listed in Tables 3 and 4. The suggested model shows good results mimicking and predicting the measured effective diffusion coefficients with relative errors of less than 50%. Only four experiments showed higher relative errors for which the correlation shows insufficient accuracy. The high error with the saturated samples is subject to stronger uncertainties in the experimental procedure and, therefore, the relative error may not be representative. The remaining remarkable deviations were samples measured at the experimental matrix’s higher boundaries and exceeding these conditions. Furthermore, the binary diffusion coefficient is overestimated for these cases; therefore, the coefficient is higher than observed. Regarding the significant deviation of 615% for sample H, the temperature is located at the upper boundary, the pressure exceeds the upper limit, and the permeability is the lowest of the entire measurement series. In this region, the model reaches its limitations. In these circumstances, additional experiments could lead to improved tuning within this region. Nevertheless, the correlation shows promising results for typical storage conditions within the European Union regarding temperature, pressure, and petrophysical properties.

In comparison with the developed correlation, model FMQ indicates higher relative errors. Here, deviations of more than 100 % can be regularly observed. Therefore, the developed correlation seems to give more accurate results. Remarkable are high errors within model FMQ’s low temperature and pressure region. Within this region, Fuller’s

method is stated to be accurate, which could indicate inaccurate modelling of the tortuosity factor of the investigated rock samples with Millington & Quirk.

### 3 Validation of Numerical Implementation by Reproduction of Experimental Results

To predict the mixing effects governed by molecular diffusion on larger scales, the experiments are reproduced within numerical simulations of the transport process in porous media. Here, the open-source simulator DuMu<sup>x</sup> is used, which has been in development by the University of Stuttgart (Institute of Modelling Hydraulic and Environmental Systems) since 2007 (Koch et al. 2020; Flemisch et al. 2011). It is based on the numeric framework DUNE (Bastian et al. 2021; Sander 2021) and is provided as an additional module to model the reactive fluid flow in porous media. DuMu<sup>x</sup> is the abbreviation for 'DUNE for Multi-{Phase, Component, Scale, Physics, ...} flow and transport in porous media'. In the past, the simulator has provided good results reproducing investigations on the lab scale (Feldmann et al. 2020), but also the simulation on field-scale, such as UHS scenarios, led to promising outcomes (Hagemann 2018; Hogeweg et al. 2022).

#### 3.1 Simulation Model

In this study, the model considers the two-phase n-component flow, including advective and diffusive transport in porous media. The simulation model is developed to describe unique processes during hydrogen storage in the subsurface. Adaptations are considered, such as within the fluid system and implementing geo- and biochemical reactions (Hogeweg and Hagemann 2022) caused by the insertion of hydrogen. However, these reactions do not occur in the present study. Here, only a calibration of the diffusive flux was done for consecutive field-scale simulations.

##### 3.1.1 Fluid System

The fluid system is composed of one phase (gas) with two components ( $H_2$  and  $CH_4$ ), which can be expanded by additional phases and components with respect to potential UHS scenarios. The gas density is modelled by Peng and Robinson (1976) to consider the compressibility of the gaseous phase in dependency of pressure and temperature. Furthermore, the dynamic viscosity of the gaseous phase is described by a combination of Stiel and Thodos (1961) and Lohrenz et al. (1964), whereby the impact of viscosity differences is expected to be small due to the minuscule pressure gradients in this study. To integrate the observations from the laboratory into the fluid system, the developed correlation of the bulk diffusion coefficient (Eq. 10-16) is implemented and, additionally, the diffusivity (fluid-matrix-interactions) is adapted to the corresponding one of the tortuosity factor (Eq. 8-9).

##### 3.1.2 Spatial Discretisation

For the spatial discretisation, representing the core sample ( $\approx 6$  cm) between the two chambers, a one-dimensional grid with 100 equidistant elements is defined. While the first

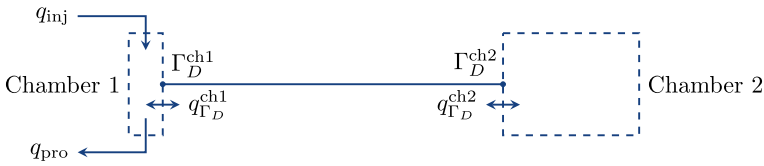


Fig. 7 Schematic representation of the domain including the modelling of the chambers

chamber possesses a relative large volume, the second chamber represents only the gas distribution element. An extrusion factor corresponding to its area is introduced to consider the axial cross section of the rock specimen. For the discretisation method, the box method (control volume finite element method) is selected due to its versatile possibilities of evaluating gradients locally. The porosity and permeability of the domain are defined homogeneously and parameterised with the measured values from the laboratory.

### 3.1.3 Initialisation and Boundary Conditions

With respect to the initialisation of the system, all elements contain only gas, which is composed entirely of hydrogen following the experimental procedure. The pressure and temperature are defined as the experimental conditions.

To model the two chambers at the sides of the core sample (cf. Fig. 7), time-dependent Dirichlet boundaries are used to mimic the changing concentrations of hydrogen and methane within the chambers. The time-dependent Dirichlet boundaries are updated explicitly in every timestep. Based on the substance present in a chamber (cf. Eq. 23), the molar concentration can be determined by Eq. 24.

$$pV = nRTZ \tag{23}$$

$$c^k = \frac{n^k}{\sum_{\kappa} n^{\kappa}} \tag{24}$$

where  $p$  is the pressure in Pa,  $V$  is the volume of the chamber in  $m^3$ ,  $n$  is the amount of substance in mol,  $R$  is the universal gas constant in  $J/(K \cdot mol)$ ,  $Z$  is the compressibility factor, and  $c^k$  is the concentration of component  $k$ .

The concentration change in the chambers is determined by a material balance for each chamber of the previous and current timestep (Eq. 25).

$$n_t^k = n_{t-1}^k - \frac{dn^k}{dt} \Delta t \tag{25}$$

where  $t$  denotes the new time,  $t - 1$  corresponds to the previous timestep, and  $\Delta t$  is the timestep size in s. The change in substance over time is thereby influenced by the flux over the boundary and additional injection/production in/from the chamber.

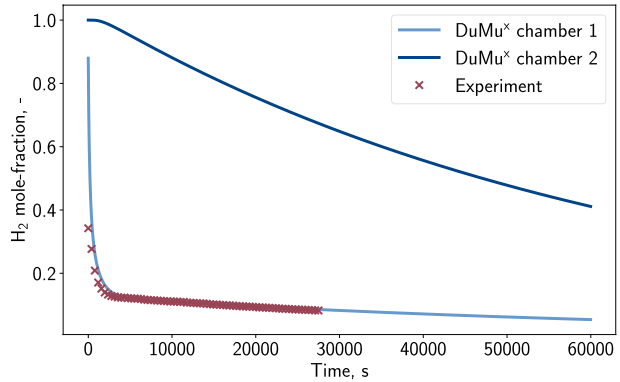
$$\frac{dn^k}{dt} = q_{\Gamma_D}^k + q_{inj}^k - q_{pro}^k \tag{26}$$

where  $q_{\Gamma_D}$  is the flux over the Dirichlet boundary in mol/s and  $q_{inj}$  and  $q_{prod}$  are the injection and production rates from a chamber in mol/s. The boundary flux can be obtained implicitly with:

**Table 5** Overview of the definition of the primary variables of the Dirichlet boundaries for chamber 1 and 2

Pri. variables	Chamber 1	Chamber 2
$p_g$	$p_{init} = p_{exp}$	$p_{init} = p_{exp}$
$S_w$	0	0
$c_g^k$	$c_{ch1,t}^k = \frac{n_{ch1,t-1}^k - (q_{\Gamma_D}^k + q_{inj}^k - q_{pro}^k)\Delta t}{\sum_k n_{ch1,t-1}^k - (q_{\Gamma_D}^k + q_{inj}^k - q_{pro}^k)\Delta t}$	$c_{ch2,t}^k = \frac{n_{ch2,t-1}^k - q_{\Gamma_D}^k \Delta t}{\sum_k n_{ch2,t-1}^k - q_{\Gamma_D}^k \Delta t}$

**Fig. 8** Comparison of hydrogen fractions versus time observed in laboratory and modelled in DuMu<sup>x</sup> for the reference sample at reference conditions ( $T = 40$  °C and  $p = 100$  bar)



$$q_{\Gamma_D}^k = \underbrace{\left( c_g^k \frac{Kk_{rg}}{\mu_g} \nabla p \right)}_{\text{advective flux}} + \underbrace{\left( D_{pm}^{k,eff} \nabla c_g^k \right)}_{\text{diffusive flux}} \hat{\rho}_g A \tag{27}$$

where  $K$  is the absolute permeability in  $m^2$ ,  $k_{rg}$  is the relative permeability (*here*:  $k_{rg} = 1$  due to single-phase gas flow),  $\mu_g$  is the dynamic viscosity of the gaseous phase in  $Pa \cdot s$ ,  $\hat{\rho}_g$  is the molar density in  $mol/m^3$ , and  $A$  is the extruded cross section area in  $m^2$ .

Concerning the first chamber, where a continuous injection of methane and production of the gas mixture occurs, the contribution to the gas composition is summarised in Eqs. (28–29). For the production composition, the concentration of the previous timestep is selected to simplify the numerical model. However, one limitation is that the maximum timestep size directly depends on the volume of the tiny chamber 1 and the rate of the continuous flushing and is therefore set to 20 s in the present study.

$$q_{inj}^k = c_{inj}^k q_{flush} \tag{28}$$

$$q_{pro}^k = c_{ch1,t-1}^k q_{flush} \tag{29}$$

where  $c_{inj}$  is the injection composition (*here*: only methane),  $q_{flush}$  is the continuous production and injection rate in  $mol/s$ ,  $c_{ch1,t-1}^k$  is the concentration in chamber 1 of the previous timestep.

A summary of the boundary definition can be found in Table 5.

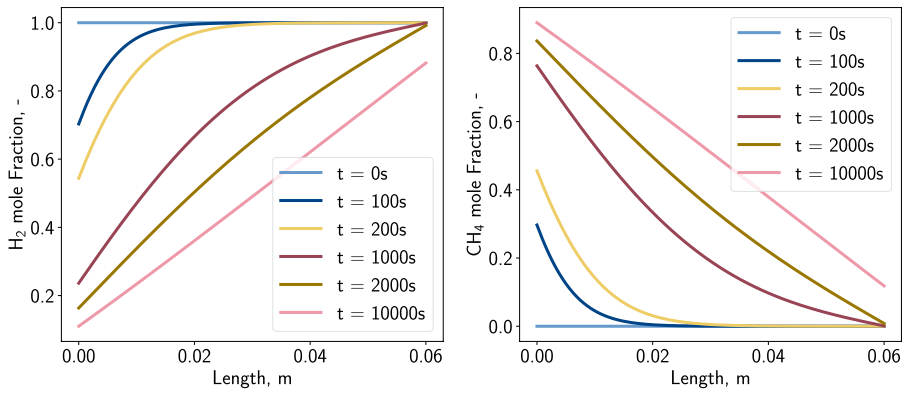


**Fig. 9** Spatial distribution of hydrogen and methane concentration within the first 10000 s

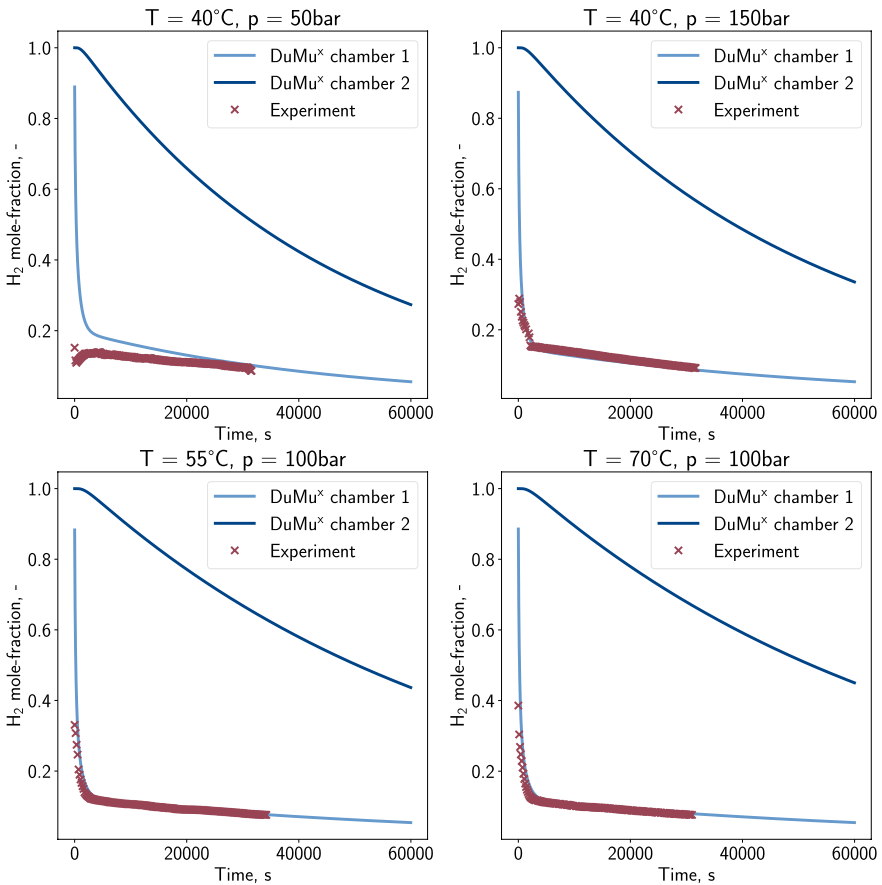


**Fig. 10** Hydrogen concentration versus time for four selected cases of sample A (Bentheimer) at different thermodynamic conditions



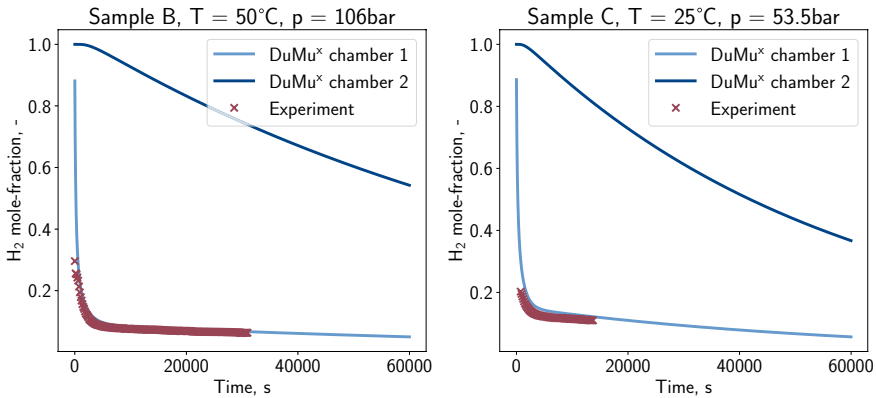


Fig. 11 Hydrogen concentration versus time for two arbitrary samples from actual storage formations

### 3.2 Results and Comparison of Numerical Simulation with the Laboratory Observations

Figure 8 compares the simulated and measured results of the reference case. The general matching parameter is the hydrogen concentration in the gas stream from chamber 1. It is evident that in the beginning, the initial hydrogen in chamber 1 is displaced by methane, leading to a rapid drop in the hydrogen concentration. Generally speaking, the higher the hydrogen concentration in chamber 1, the higher the flux of molecular diffusion. Regarding the quality of the match between observed and modelled data, the implementation in DuMu<sup>x</sup> shows similar hydrogen concentrations and a congruent slope in dependency of time. Based on the simulations, it is also possible to evaluate the spatial distribution of the gas composition within the core sample as depicted in Fig. 9. Again, the simultaneous decrease in the hydrogen concentration and increase in methane content can be observed. For this specific case, the first influence of methane in the second chamber is remarkable after approximately 2000 s, with a continuously increasing trend.

The quality of the correlations and implementation is evaluated at different thermodynamic conditions. Figure 10 depicts measurements at typical storage conditions. The first case ( $T = 40\text{ °C}$  and  $p = 50\text{ bar}$ ) shows a deviation, which is expected due to the high relative error of  $\delta_{D_{pm}^{AB}} \approx 50\%$  of the correlation. For the other three cases, the modelling of the experiments yields congruent and satisfying results. Similar qualities of match with minor variance can be observed for the samples from actual storage formations (cf. Fig. 11).

In general, implementing the developed correlation in DuMu<sup>x</sup> permits a good reproduction of the laboratory experiments. Deviations between the modelled and observed results are mainly caused by inaccuracies in the developed correlation.

## 4 Conclusions

With hydrogen injection in former gas fields or storage formations, the prediction of mixing behaviour with the initial gas becomes important. In this study, a combination of correlations describing the bulk diffusion and the tortuosity factor of the rock specimen was developed based on performed laboratory experiments on various samples at the range of

typical reservoir conditions. Compared to existing models, the proposed correlation yields lower relative errors for the measured results and showed only some exceptions within the range of more than 100 %. Although weaknesses could be observed regarding combinations of high pressure and temperature, the proposed model shows accurate results for typical storage rocks with a wide range of porosity and permeability ( $17\% < \phi < 32\%$  and  $17 \text{ mD} < k < 2500 \text{ mD}$ ). However, whether the developed model applies to other rock types, such as tight sandstones and shale, is questionable as pore connectivity may vary, and further processes (e.g. adsorption at rock surface) may become significant. The limitations regarding thermodynamic conditions are  $10 \text{ bar} < p < 200 \text{ bar}$  and  $25 \text{ }^\circ\text{C} < T < 100 \text{ }^\circ\text{C}$ . Further experiments conducted in extreme thermodynamic environments could lead to improved results and extend the correlations. Measurements of additional gas compositions could be used for a more general description of the bulk diffusion coefficients and experiments addressing the tortuosity factor of the specimen could also mitigate remaining uncertainty of the model.

The implementation of the developed correlations into the open-source simulator DuMu<sup>x</sup> allowed the reproduction of the observed data within the accuracy of the correlation. Here, the adaptability of the source code allowed a straightforward implementation of the correlation and the experimental procedure, which might be limitations in other simulators. The extension of the simulation model can be used to predict the impact of molecular diffusion during hydrogen storage in the subsurface. Nevertheless, the transfer from laboratory-scale to the field-scale should be verified empirically based on actual field data.

**Author Contributions** SH wrote and proof-read this manuscript, developed, implemented, and visualised the presented material. JM contributed with the collection of the experimental data and writing parts of the manuscript. BH conceptualised, supervised this work, and supported with proof-reading the manuscript. LG supported with supervision and reviewing of the manuscript.

**Funding** Open Access funding enabled and organized by Projekt DEAL. This project has received funding from the Fuel Cells and Hydrogen 2 Joint Undertaking (now Clean Hydrogen Partnership) under grant agreement No 101006632. This Joint Undertaking receives support from the European Union's Horizon 2020 research and innovation programme, Hydrogen Europe and Hydrogen Europe Research. Additionally, some results have been produced in cooperation with DMT GmbH & Co. KG, and we acknowledge funding by TÜV Nord AG.

**Data Availability** The datasets of the laboratory experiments analysed during the current study are available in the HyUSPRE repository, Michelsen et al. (2023).

**Code Availability** The implementation in the open-source simulator DuMu<sup>x</sup> is available in its persistent form in the repository, Hogeweg et al. (2023).

## Declarations

**Conflict of interest** The authors have no relevant financial or non-financial interests to disclose.

**Open Access** This article is licensed under a Creative Commons Attribution 4.0 International License, which permits use, sharing, adaptation, distribution and reproduction in any medium or format, as long as you give appropriate credit to the original author(s) and the source, provide a link to the Creative Commons licence, and indicate if changes were made. The images or other third party material in this article are included in the article's Creative Commons licence, unless indicated otherwise in a credit line to the material. If material is not included in the article's Creative Commons licence and your intended use is not permitted by statutory regulation or exceeds the permitted use, you will need to obtain permission directly from the copyright holder. To view a copy of this licence, visit <http://creativecommons.org/licenses/by/4.0/>.

## References

- Bastian, P., Blatt, M., Dedner, A., Dreier, N.-A., Engwer, C., Fritze, R., Gräser, C., Grüninger, C., Kempf, D., Klöforn, R., Ohlberger, M., Sander, O.: The dune framework: basic concepts and recent developments. *Comput. Math. Appl.* **81**, 75–112 (2021). <https://doi.org/10.1016/j.camwa.2020.06.007>
- Bear, J.: Modeling phenomena of flow and transport in porous media. Theory and Applications of Transport in Porous Media, vol. 31. Springer, Cham (2018). <https://doi.org/10.1007/978-3-319-72826-1>
- Brooks, R.H., Corey, A.T.: Hydraulic properties of porous media and their relation to drainage design. *Transact. ASAE* **7**(1), 0026–0028 (1964). <https://doi.org/10.13031/2013.40684>
- Brown, R.: Xxvii. A brief account of microscopical observations made in the months of june, july and august 1827, on the particles contained in the pollen of plants; and on the general existence of active molecules in organic and inorganic bodies. *Philoso. Mag.* **4**(21), 161–173 (1828). <https://doi.org/10.1080/14786442808674769>
- Chen, L.L.-Y., Katz, D.L., Tek, M.R.: Binary gas diffusion of methane-nitrogen through porous solids. *AIChE J.* **23**(3), 336–341 (1977). <https://doi.org/10.1002/aic.690230317>
- Darcy, H.: Les Fontaines Publiques de La Ville de Dijon: Exposition et Application Des Principes à Suivre et Des Formules à Employer Dans Les Questions de Distribution D'eau: Ouvrage Terminé Par Un Appendice Relatif Aux Fournitures D'eau de Plusieurs Villes, Au Filtrage Des Eaux et à La Fabrication Des Tuyaux de Fonte, de Plomb, de Tôle et de Bitume. Les Fontaines Publiques de La Ville de Dijon: Exposition et Application Des Principes à Suivre et Des Formules à Employer Dans Les Questions de Distribution d'eau : Ouvrage Terminé Par Un Appendice Relatif Aux Fournitures d'eau de Plusieurs Villes, Au Filtrage Des Eaux et à La Fabrication Des Tuyaux de Fonte, de Plomb, de Tôle et de Bitume. Victor Dalmont, Paris (1856)
- Feldmann, F., Strobel, G.J., Masalmeh, S.K., AlSumaiti, A.M.: An experimental and numerical study of low salinity effects on the oil recovery of carbonate rocks combining spontaneous imbibition, centrifuge method and coreflooding experiments. *J. Petrol. Sci. Eng.* **190**, 107045 (2020). <https://doi.org/10.1016/j.petrol.2020.107045>
- Einstein, A.: über die von der molekularkinetischen theorie der wärme geforderte bewegung von in ruhenden flüssigkeiten suspendierten teilchen. *Ann. Phys.* **322**(8), 549–560 (1905). <https://doi.org/10.1002/andp.19053220806>
- Fick, A.: Ueber diffusion. *Annalen der Physik und Chemie* **170**(1), 59–86 (1855). <https://doi.org/10.1002/andp.18551700105>
- Fuller, E.N., Giddings, J.C.: A comparison of methods for predicting gaseous diffusion coefficients. *J. Chromatogr. Sci.* **3**(7), 222–227 (1965). <https://doi.org/10.1093/chromsci/3.7.222>
- Fuller, E.N., Ensley, K., Giddings, J.C.: Diffusion of halogenated hydrocarbons in helium. The effect of structure on collision cross sections. *J. Phys. Chem.* **73**(11), 3679–3685 (1969). <https://doi.org/10.1021/j100845a020>
- Fuller, E.N., Schettler, P.D., Giddings, Calvin J.: New method for prediction of binary gas-phase diffusion coefficients. *Ind. Eng. Chem.* **58**(5), 18–27 (1966). <https://doi.org/10.1021/ie50677a007>
- Flemisch, B., Darcis, M., Erbertseder, K., Faigle, B., Lauser, A., Mosthaf, K., Müthing, S., Nuske, P., Tatomir, A., Wolff, M., Helmig, R.: Dumux: Dune for multi-(phase, component, scale, physics,...) flow and transport in porous media. *Adv. Water Resour.* **34**(9), 1102–1112 (2011). <https://doi.org/10.1016/j.advwatres.2011.03.007>
- Guevara-Carrion, G., Ancherbak, S., Mialdun, A., Vrabec, J., Shevtsova, V.: Diffusion of methane in supercritical carbon dioxide across the widom line. *Sci. Rep.* **9**(1), 8466 (2019). <https://doi.org/10.1038/s41598-019-44687-1>
- Hagemann, B.: Numerical and Analytical Modeling of Gas Mixing and Bio-Reactive Transport During Underground Hydrogen Storage, 1. auflage edn. Schriftenreihe Des Energie-Forschungszentrums Niedersachsen, vol. Band 50. Cuvillier Verlag, Göttingen (2018)
- Helmig, R.: Multiphase flow and transport processes in the subsurface. Environmental Engineering. Springer, Berlin, New York (1997)
- Hogeweg, S., Hagemann, B.: Integrated modeling approach for the overall performance, integrity, and durability assessment of hydrogen storage at the reservoir and near-wellbore scale. Technical report, Clausthal University of Technology (2022)
- Hogeweg, S., Michelsen, J., Hagemann, B., Ganzer, L.: Replication Data for: empirical and numerical modelling of gas-gas diffusion for binary hydrogen-methane systems at underground gas storage conditions. GRO.data (2023). <https://doi.org/10.25625/YVCV2Y>
- Hogeweg, S., Strobel, G., Hagemann, B.: Benchmark study for the simulation of underground hydrogen storage operations. *Comput. Geosci.* **26**(6), 1367–1378 (2022). <https://doi.org/10.1007/s10596-022-10163-5>

- Koch, T., Gläser, D., Weishaupt, K., Ackermann, S., Beck, M., Becker, B., Burbulla, S., Class, H., Coltman, E., Emmert, S., Fetzer, T., Grüniger, C., Heck, K., Hommel, J., Kurz, T., Lipp, M., Mohammadi, F., Scherrer, S., Schneider, M., Seitz, G., Stadler, L., Utz, M., Weinhardt, F., Flemisch, B.: Dumux 3-an open-source simulator for solving flow and transport problems in porous media with a focus on model coupling. *Comput. Math. Appl.* (2020). <https://doi.org/10.1016/j.camwa.2020.02.012>
- Lohrenz, J., Bray, B.G., Clark, C.R.: Calculating viscosities of reservoir fluids from their compositions. *J. Petrol. Technol.* **16**(10), 1171–1176 (1964). <https://doi.org/10.2118/915-PA>
- Michelsen, J., Langanke, N., Hagemann, B., Hogeweg, S., Ganzer, L.: Diffusion measurements with hydrogen and methane through reservoir rock samples. In: *Advanced SCAL for Carbon Storage & CO2 Utilization*, Abu Dhabi (2023)
- Michelsen, J., Thaysen, E.M., Hogeweg, S., Hagemann, B., Hassanpouryouzband, A., Langanke, N., Edlmann, K., Ganzer, L.: Hydrogen reservoir flow behaviour: Measurements of molecular diffusion, mechanical dispersion and relative permeability. H2020 hyuspre project report, Clausthal University of Technology (2023)
- Michelsen, J., Thaysen, E.M., Hogeweg, S., Hagemann, B., Hassanpouryouzband, A., Langanke, N., Edlmann, K., Ganzer, L.: Data for: HyUSPRE - Work Package 4 - Hydrogen Reservoir Flow Behaviour: Measurements of Molecular Diffusion, Mechanical Dispersion and Relative Permeability. GRO.data (2023). <https://doi.org/10.25625/7XCCL8>
- Millington, R.J., Quirk, J.P.: Permeability of porous solids. *Trans. Faraday Soc.* **57**, 1200 (1961). <https://doi.org/10.1039/tf9615701200>
- Pandey, G.N., Tek, M.R., Katz Donald, L.: Diffusion of fluids through porous media with implications in petroleum geology. *Am. Asso. Petrol. Geol. Bull.* **58**(2), 291–303 (1974). <https://doi.org/10.1306/83d913da-16c7-11d7-8645000102c1865d>
- Peng, D.-Y., Robinson, D.B.: A new two-constant equation of state. *Ind. Eng. Chem. Fundam.* **15**(1), 59–64 (1976). <https://doi.org/10.1021/i160057a011>
- Poling, B.E., Prausnitz, J.M., O'Connell, J.P.: *The Properties of Gases and Liquids*, 5th, ed McGraw-Hill, New York (2001)
- Sander, O.: *DUNE - The Distributed and Unified Numerics Environment*. Springer, S.I. (2021)
- Stiel, L.I., Thodos, G.: The viscosity of nonpolar gases at normal pressures. *AIChE J.* **7**(4), 611–615 (1961). <https://doi.org/10.1002/aic.690070416>
- Von Smoluchowski, M.: Zur kinetischen theorie der brownischen molekularbewegung und der suspensionen. *Ann. Phys.* **326**(14), 756–780 (1906). <https://doi.org/10.1002/andp.19063261405>
- Wicke, E., Kallenbach, R.: Die oberflächendiffusion von kohlendioxid in aktiven kohlen. *Kolloid-Zeitschrift* **97**(2), 135–151 (1941). <https://doi.org/10.1007/BF01502640>
- Wilke, C.R., Lee, C.Y.: Estimation of diffusion coefficients for gases and vapors. *Ind. Eng. Chem.* **47**(6), 1253–1257 (1955). <https://doi.org/10.1021/ie50546a056>

**Publisher's Note** Springer Nature remains neutral with regard to jurisdictional claims in published maps and institutional affiliations.